Korean J. Chem. Eng., 36(11), 1826-1838 (2019)
DOI: 10.1007/s11814-019-0400-1

pISSN: 0256-1115
eISSN: 1975-7220

Process optimization and synthesis of lanthanum-cobalt perovskite type nanoparticles ($LaCoO_3$) prepared by modified proteic method: Application of response surface methodology

Zaharaddeen N. Garba*,, Wei Xiao*, Weiming Zhou*, Ibrahim Lawan*, Yifan Jiang*, Mingxi Zhang*, and Zhanhui Yuan*,†**

*College of Materials Science and Engineering, Fujian Agriculture and Forestry University, Fuzhou, Fujian Province, China
**Department of Chemistry, Ahmadu Bello University Zaria, Nigeria
(*Received 5 July 2019 • accepted 8 October 2019*)

Abstract−Due to increasing interest in the application of perovskites as promising adsorbents, the present study looks at how central composite design (CCD), a subset of response surface methodology (RSM), can statistically play a role in producing optimum lanthanum oxide-cobalt perovskite type nanoparticles ($LaCoO_3$) by using a modified proteic synthesis method. The optimum $LaCoO_3$ produced was tested for its capability in removing methyl orange (MO) and rhodamine B (RhB) dyes from aqueous solution. Calcination temperature and calcination time were optimized with the responses being percentage yield, MO and RhB removal. The best temperature and calcination time obtained were 775 °C and 62 mins, respectively, giving good and appreciable values for the three responses. The resulting optimal $LaCoO_3$ was characterized by Fourier transform infra-red (FTIR), ultraviolet-visible spectrophotometry (UV/vis), scanning electron microscopy (SEM), pH of zero point charge (pH_{pzc}) as well as BET analysis, yielding a mesoporous adsorbent with surface area of 61.130 $m^2 g^{-1}$ as well as 223.55 and 239.45 mg g^{-1} as the monolayer adsorption capacity values for MO and RhB, respectively. Freundlich model was the best in describing the equilibrium adsorption data with respect to both MO and RhB with the kinetic data for the two dyes both obeying pseudo-second-order kinetics model.

Keywords: $LaCoO_3$, Perovskite, Modified Proteic Method, Adsorption, Methyl Orange, Rhodamine B

INTRODUCTION

The growing use of dyes which are classified as hazardous compounds has recorded a significant increase in recent years due to their wide range of industrial applications. They are mostly used in various industrial processes, such as paper and pulp manufacturing, plastics, dyeing of clothes, leather treatment and printing, which later results in soil and water contamination due to the presence of industrial effluents containing dyes [1,2]. The presence of these dyes is unwanted in the environment due to their toxicity, with most of them being recalcitrant to microbial degradation. Some of the dyes also lead to the formation of compounds that are potentially carcinogenic due to their ability of undergoing anaerobic degradation [3]. Another threat posed by the presence of dyes in the environment is that the highly colored wastewaters they form may impede sunlight and oxygen from reaching various aquatic organisms, which leads to their demise [4].

Acid, basic and azo are the major classes of dyes with chromophore groups being responsible for the observed color of azo dyes [5,6]. An example of hazardous azo dye is methyl orange (MO). It exhibits high toxicity with the potential of generating carcinogenic metabolites despite the favorable dying properties it possesses [7]. Another dye classified as hazardous and harmful to human health is Rhodamine B (RhB). Due to the potential for RhB to be carcinogenic, California authorities required a warning label on all products containing it [8]. Hence, it is very imperative to monitor and control how these dyes get into water systems. The most popular, effective and easy to handle technique widely employed for the removal of dyes and other contaminants from contaminated water is adsorption, as it is capable of removing high percentage of dyes over a wide concentration range [9-12].

Perovskites with a general formula ABO_3 are classified as mixed oxide ceramic materials with metal ions having large atomic radii (mostly lanthanum) and smaller atomic radii (mostly transition metals) occupying the A and B positions, respectively. These perovskite materials are reported as promising adsorbents which are applied in the removal of various adsorbates such as pesticides, volatile organic compounds and dyes [13,14]. Several researchers reported perovskites and other self-assembled nanostructures and nanocomposites to be versatile materials which are synthesized easily, thereby exhibiting diverse properties [15-21]. Various factors such as the synthetic route as well as the metal type occupying the B site play a key role on how efficient a perovskite material can be for specific applications [22]. Various methods, such as co-precipitation, pechini and solgel method among others were reported to be employed for the synthesis of perovskite materials [15-17]. Too achieve the perovskite phase formation, high temperature treatments are very crucial after the initial synthesis steps [23].

Economic viability and efficacy of output are among the numerous objectives of researches in science and engineering. Experimental

†To whom correspondence should be addressed.
E-mail: zhanhuiyuan@fafu.edu.cn

Table 1. Characteristics of methyl orange (MO) and rhodamine B (RhB) dyes

Name	Chemical formula	Formula weight (g mol^{-1})	Color	Form	pka	λ_{max}
MO	$C_{14}H_{14}N_3NaO_3S$	327.33	Yellow-Orange	Powder/Solid	3.4	464
Rhd B	$C_{28}H_{31}ClN_2O_3$	479.02	Green	Solid	3.7	553

design techniques play a vital role to researchers in terms of rationalizing experiments, which helps in reducing cost as well as lessening the adversity often experienced by researchers. Response surface methodology (RSM) is one such statistical tool that is very crucial as reported by many researchers in the preparation of adsorbent materials as well as optimizing the adsorption conditions [24-27].

We noticed several published articles suggesting the potentials of perovskites type nano particles as adsorbent; however, we did not come across any published article that reported the role central composite design (CCD) can play in producing an optimum perovskite nanoparticle type for the adsorption of dyes, specifically methyl orange (MO) and rhodamine B (RhB). CCD is a technique (subset of RSM) that does not require much experimentation in probing the extent of influence exerted by the parameters to be optimized. Another added advantage of CCD is its ability to trim experiments that are inconsequential as well as checkmate the possibility of synergy existing amongst the factors.

Therefore, this article is aimed at evaluating the role of CCD in optimizing the paramount parameters (calcination temperature and time) involved in producing lanthanum-cobalt perovskite type nanoparticles by employing a facile method for an effective adsorption of MO and RhB dyes, which is, to the best of our knowledge, the first time such a work is being reported.

EXPERIMENTAL SECTION

1. Reagents

The reagents employed in this work include La_2O_3, HNO_3, $Co(NO_3)_2$ and soy protein as complex agent. Adsorbates used were methyl orange (MO) and rhodamine B (RhB) dyes with their characteristics summarized in Table 1. Stock solutions of the dyes were prepared by dissolving 1 g of the respective dyes in 1 L volumetric flask (1,000 mg L^{-1}) concentration which was diluted to the required concentrations using de-ionized water. All chemicals used were of analytical grade supplied by Aladdin Industrial Corporation and Shanghai Macklin Biochemical Co ltd Shanghai, China which were used without further purification. La_2O_3 was dissolved in nitric acid to form lanthanum nitrate.

2. Synthesis of the Lanthanum Oxide-cobalt Perovskite Type Nanoparticle

The synthesis method of $LaCoO_3$ perovskite-type nanoparticle in this work was the modified proteic method reported by Santos et al. [22] with further modification. The starting materials we used were cobalt and lanthanum nitrates which were mixed with a complexing agent (soy protein) [22]. The method involved dissolving the appropriate amount of cobalt (II) nitrate in distilled water by magnetic stirring at 30 °C for half an hour, which was followed by the addition of a given amount of lanthanum (III) nitrate and kept under stirring for another 30 mins. The solution temperature was then raised to 70 °C, followed by introducing soy protein into the system, thereby maintaining the temperature at 70 °C for 1 h, which resulted in a viscous system. The temperature was further raised to 250 °C under close monitoring with 10 °C min^{-1} set as the heating rate until the formation of a precursor powder. The precursor was then calcinated at various temperatures and time as designed by the RSM software (Table 2).

2-1. Modification

The original procedure reported by [22] was further modified here to suit our objective. The modifications involved incorporating cobalt nitrate among our starting materials as well as designing a set of

Table 2. Experimental design matrix from CCD with two experimental variables and three responses

Run no.	Temperature (°C)		Time (mins)		Responses (%)					
	β_1		β_2		Yield (Y_1)		MO (Y_2)		RhB (Y_3)	
	Coded	Actual	Coded	Actual	Observed	Predicted	Observed	Predicted	Observed	Predicted
1	−1	644	−1	43	20.06	19.35	84.55	81.84	71.21	71.34
2	+1	856	−1	43	25.83	24.28	91.62	88.59	78.48	82.48
3	−1	644	+1	107	28.26	26.26	73.57	77.01	59.10	62.83
4	+1	856	+1	107	23.25	20.42	80.89	84.01	68.48	76.08
5	$-\alpha$	600	0	75	21.11	22.28	74.74	73.31	54.55	53.43
6	$+\alpha$	900	0	75	19.26	21.63	83.00	83.02	77.29	70.68
7	0	750	$-\alpha$	30	21.26	22.12	86.75	90.89	90.90	89.58
8	0	750	$+\alpha$	120	21.61	24.29	88.78	84.23	85.45	79.04
9	0	750	0	75	27.33	27.27	96.30	96.66	76.48	76.12
10	0	750	0	75	27.09	27.27	96.75	96.66	75.90	76.12
11	0	750	0	75	27.17	27.27	95.41	96.66	75.14	76.12
12	0	750	0	75	27.34	27.27	97.72	96.66	76.20	76.12
13	0	750	0	75	27.42	27.27	97.11	96.66	76.11	76.12

experiments using CCD (Version 8.0.6 Stat Ease, Inc., Minneapolis, MN 55413, USA of the design expert statistical software) to help us optimize the calcination temperature and calcination time. The design can be seen in Table 2.

3. CCD as Design of Experiment Tool

CCD helped us study the singular combination as well as quadratic effects exerted by the two factors optimized on the three responses. CCD is a popular second-order model employed by numerous scientists and engineers due to its suitability in analyzing interaction between preparation parameters as well as trimming unnecessary experiments. Three major operations (2^n factorial runs, 2n axial runs and 5 center runs) characterized CCD as represented below: [24,28].

$$\text{Total number of experiments}=2^n+2n+n_c \quad (1)$$

Five replicates located at center points (0, 0) were used in determining the experimental error and data reproducibility. Four factorial points were represented by +1 and −1 with ($\pm\alpha$, 0) and (0, $\pm\alpha$) describing the four axial points. The value of α can be obtained using Eq. (2) below [29]:

$$\alpha=N_p^{1/4} \quad (2)$$

where number of points in the cube portion of the design is described by $N_p=2^k$ while k is the variables amount. The optimal model predictor quadratic equation applied for the determination of the responses is expressed as:

$$Y=b_o+\Sigma_{i=1}^{n}b_{ii}\beta_i+(\Sigma_{i=1}^{n}b_{ii}\beta_i)^2+\Sigma_{i=1}^{n-1}\Sigma_{j=i+1}^{n}b_{ij}\beta_i\beta_j \quad (3)$$

Y is the response predicted, b_o stands for the constant coefficients-experimental error (measurement error on the response and unaccounted variations), b_{ii} and b_{ij} are the quadratic as well as the interaction coefficients, respectively. The variables coded values are β_i and β_j. Calcination temperature coded as β_1 and calcination time coded as β_2 were the variables studied in this work with their respective ranges chosen based on literature.

Version 8.0.6 Stat Ease, Inc., Minneapolis, MN 55413, USA of the design expert statistical software was employed for model fitting and significance for the three responses.

4. Adsorbent Characterization

The $LaCoO_3$ surface was analyzed for microstructure and elemental distribution using scanning electron microscopy, SU8010 (HITACHI) instrument. FTIR analyses (4,000 to 400 cm^{-1}) were carried out using Nicolet™ iS™ 5 spectrometer. Autosorb-iQ analyzer (Quantachrome) equipment was used in studying the surface area and pore width of the adsorbent from N_2 physisorption at −196 °C with the BET method used in calculating the specific surface area and BJH method for pore volume and pore size distribution. Shimadzu Ultraviolet-Visible spectrophotometer (UV-2500) was employed in analyzing the Co^{2+}/La^{3+} aqueous systems before and after introducing the soy protein in the scan range of 200-800 nm.

5. Adsorption Isotherms

Two-parameter (Langmuir Freundlich and Temkin) as well as three-parameter (Sips and Toth) isotherms were applied to fit the equilibrium data for the adsorption of MO and RhB dyes. They are mathematically described as:

$$\frac{C_e}{q_e}=\frac{1}{K_L\cdot Q_a^0}+\frac{C_e}{Q_a^0} \quad (4)$$

$$\log q_e=\log K_F+\frac{1}{n}\log C_e \quad (5)$$

$$q_e=\frac{RT}{b}\ln A+\frac{RT}{b}\ln C_e \quad (6)$$

$$\ln\left(\frac{q_e}{q_m-q_e}\right)=\frac{1}{n}\ln(C_e)+\frac{1}{n}(b_S)^{\frac{1}{n}} \quad (7)$$

$$\ln\left(\frac{q_e^n}{q_m^n-q_e^n}\right)=n_t\ln(C_e)+n_t\ln(K_t) \quad (8)$$

where C_e (mg L^{-1}) is the equilibrium concentration of the adsorbates, q_e stands for the adsorbate amount adsorbed per unit adsorbent weight, while Q_a^0 (mg g^{-1}) and K_L (L mg^{-1}) are Langmuir constants related to maximum adsorption capacity and rate of adsorption, respectively, K_F (mg^{1-n} g^{-1} L^n) is the adsorption capacity when the adsorbate equilibrium concentration is equal to 1.00 mg L^{-1} [30] with n related to adsorption intensity [31]. In general, n>1 suggests that adsorbate is favorably adsorbed on the adsorbent. The higher the n value, the stronger the adsorption intensity. A (L g^{-1}) and (RT/b)=B (J mol^{-1}) are Temkin constants, which are related to heat of sorption and maximum binding energy, respectively, b_S is the Sips isotherm constant related to energy of adsorption, K_t is the Toth model adsorption isotherm constant [32], R is the gas constant (8.31 J mol^{-1} K^{-1}) and T (K) is the absolute temperature.

Dimensionless separation factor, R_L, is essential characteristic of the Langmuir equation defined as [33]:

$$R_L=\frac{1}{1+K_LC_o} \quad (9)$$

where C_o is the highest initial solute concentration. R_L values indicate whether the adsorption is unfavorable (R_L>1), linear (R_L=1), favorable (0<R_L<1), or irreversible (R_L=0).

6. Adsorption Equilibrium and Kinetic Studies

Batch adsorption was carried out in a set of Erlenmeyer flasks (250 mL) for the removal efficiency of MO and RhB in aqueous solution. 0.1 g of the $LaCoO_3$ was added into the dye solutions, which were placed in an isothermal shaker at a fixed speed of 180 rpm and varying temperatures (30 °C, 40 °C and 50 °C) to reach equilibrium state. The samples were filtered afterwards to separate adsorbents from the adsorbates. Ultraviolet-Visible (UV 2500) spectrophotometer was used in determining the remaining concentrations of the adsorbates at their respective wavelengths of 464 and 553 nm for MO and RhB, respectively. The amount adsorbed at equilibrium, q_e (mg g^{-1}) was calculated as:

$$q_e=\frac{(C_o-C_e)V}{W} \quad (10)$$

V (L) is the volume of the solution, and W (g) is the weight of the adsorbent used.

The percentage removal of the adsorbates was calculated as:

$$\text{Dyes removal (\%)}=\frac{C_o-C_e}{C_o}\times 100 \quad (11)$$

Concentration of the dyes (MO and RhB) solution was determined at varying time intervals to have an idea about the adsorption process kinetics. The amounts of MO and RhB adsorbed at time t, q_t (mg g^{-1}) were calculated using Eq. (12):

$$q_t = \frac{(C_o - C_t)V}{W} \quad (12)$$

Pseudo-first-order, pseudo-second-order and intra-particle diffusion kinetic models were investigated to determine the order of the process and the adsorption mechanism.

The solution pH was adjusted to study the effect of initial pH (2-12) on the dyes adsorption. The reagents used for the solution pH adjustments were 0.1 M HCl and 0.1 M KOH solutions. The final pH of the solutions was measured using a pH meter (Martini instrument, Mi 106) a fixed initial concentration (100 mg L^{-1}) adsorbent dosage 0.10 g) and temperature (30 °C) until equilibrium was established. The % R was calculated using Eq. (9).

The pH_{pzc} was determined by adopting solid addition method similar to the method reported by [34,35]. The method involved addition of adsorbent sample (0.1 g) into 100 mL conical flasks containing 50 mL of various concentrations of KNO_3 (0.1, 0.01, 0.001 mol dm^{-3}). To adjust the initial pH of the KNO_3 solution from 2-12, 0.1 M KOH and HCl were used. The sample was shaken for at 180 rpm until equilibrium was established, then the final pH was recorded. The final pH was plotted against initial pH values of the solution with plateau point on the plot noted and recorded as the pH_{pzc} of the $LaCoO_3$ [34].

7. Desorption Studies

The dyes (MO and Rhd B) were adsorbed onto $LaCoO_3$ at a concentration of 100 mg L^{-1} until equilibrium was reached. The $LaCoO_3$ were then filtered out and dried at 60 °C. The method of [36] was then employed for the regeneration studies with slight modification. The efficiency was determined as:

$$\text{Desorption efficiency (\%)} = \frac{C_{de}}{C_{ad}} \times 100 \quad (13)$$

where C_{de} and C_{ad} are the masses of dyes desorbed and adsorbed, respectively.

RESULTS AND DISCUSSION

1. Development of Regression Model Equation

Table 2 presents the range of variables considered for $LaCoO_3$ preparation with three responses coded as Y_1, Y_2 and Y_3 representing percentage yield, percentage removal of MO and RhB, respectively. Upon correlation using CCD, the polynomial regression

Table 3. The ANOVA for response surface quadratic model of $LaCoO_3$ yield, MO removal and RhB removal by $LaCoO_3$

Source	Sum of squares	Degree of freedom	Mean square	F value	Prob>F
$LaCoO_3$ yield					
Model	103.40	5	20.68	4.85	0.0310
β_1	0.43	1	0.43	0.10	0.7599
β_2	4.67	1	4.67	1.10	0.3299
$\beta_1\beta_2$	29.05	1	29.05	6.81	0.0349
β_1^2	49.13	1	49.13	11.52	0.0115
β_2^2	28.74	1	28.74	6.74	0.0356
Residual	29.84	7	4.26	-	-
A.P. 5.644		**R^2 0.7760**		**Adj. $R^2$0.6160**	
MO removal					
Model	812.67	5	162.53	14.38	0.0014
β_1	94.43	1	94.43	8.36	0.0233
β_2	44.36	1	44.36	3.93	0.0880
$\beta_1\beta_2$	0.016	1	0.016	1.38×10^{-3}	0.9714
β_1^2	594.77	1	594.77	52.63	0.0002
β_2^2	143.95	1	143.95	12.74	0.0091
Residual	79.10	7	11.30	-	-
A.P. 10.225		**R^2 0.9113**		**Adj. $R^2$0.8479**	
RhB removal					
Model	931.95	5	186.39	7.39	0.0103
β_1	297.79	1	297.79	11.81	0.0109
β_2	111.14	1	111.14	4.41	0.0740
$\beta_1\beta_2$	1.11	1	1.11	0.044	0.8396
β_1^2	344.24	1	344.24	13.65	0.0077
β_2^2	116.54	1	116.54	4.62	0.0687
Residual	176.54	7	25.22	-	-
A.P. 10.59		**R^2 0.8407**		**Adj. $R^2$0.7270**	

equations developed were quadratic expressions for all the three responses. The selection of model expression was based on the highest order of polynomial, model not aliased as well as the significance of additional terms. The predicted and experimental data correlated well based on the model's R^2 values of 0.7760 (yield), 0.9113 (MO) and 0.8407 (Rhd B), which were within suitability range [37]. The R^2 values for the yield as well as percentage removals of MO and RhB were reasonable and in good agreement with adjusted R^2 (Adj. R^2) values of 0.6160, 0.8479 and 0.7270, respectively, indicating reasonable agreement between the predicted values and the actual values. Eqs. (14), (15) and (16) show the proposed equations generated by the software for the $LaCoO_3$ yield (Y_1), percentage removals of MO (Y_2) and RhB (Y_3) responses, respectively:

$$Y_1 = +27.27 - 0.23\beta_1 + 0.76\beta_2 - 2.70\beta_1\beta_2 - 2.66\beta_1^2 - 2.03\beta_2^2 \quad (14)$$

$$Y_2 = +96.66 + 3.44\beta_1 - 2.35\beta_2 + 0.06\beta_1\beta_2 - 9.25\beta_1^2 - 4.55\beta_2^2 \quad (15)$$

$$Y_3 = +76.12 + 6.10\beta_1 - 3.73\beta_2 + 0.53\beta_1\beta_2 - 7.03\beta_1^2 + 4.09\beta_2^2 \quad (16)$$

The negative and positive signs before the terms indicate antagonistic and synergetic effects of the respective variables. Uni-factor, double factor and quadratic effects are also shown by the single, two and second order variables, respectively.

2. Statistical Analysis

The analysis of variance (ANOVA) generated for the surface quadratic model in the of $LaCoO_3$ yield, percentage removals of MO and RhB is presented on Table 3. To validate the significance and adequacy of the models, ANOVA was very essential. The mean squares on each table were calculated when the sum of squares of each of the variation sources and the error variance were divided by the acquired degrees of freedom [38]. The terms from each model are thought to be significant only if Prob.>F is less than 0.05.

From Table 3, the model was deemed to be significant due to F-value of 4.85 and Prob.>F of 0.03. In this case, the significant model terms were $\beta_1\beta_2$, β_1^2 and β_2^2 on the other hand, β_1 and β_2 were insignificant to the response (Y_1). The signal-to-noise ratio is gauged by adequate precision (AP). A ratio above 4 is appropriate. In this case, an adequate signal was signified for Y_1 based on the ratio value of 5.64, which implies that the design space can be steered by this model. The model F-value and Prob.>F with respect to percentage removals of MO and RhB were 14.38, 0.0014 and 7.39, 0.0103, respectively, signifying the model's significance. The MO removal by $LaCoO_3$ model had β_1, β_1^2 and β_2^2 as significant terms, while β_1 and β_1^2 were the significant terms in the RhB model.

Both models can be used to navigate the design space based on the adequate signals of 10.225 and 10.597 shown by MO and RhB, respectively. The ANOVA results obtained show the adequacy of both models (Eqs. (14), (15) and (16)) in predicting the $LaCoO_3$ yield, percentage removals of MO and RhB respectively. Furthermore, Fig. 1(a)-(c) shows the predicted values versus the experimental values for the three responses. The figures further prove the success of these developed models in effectively correlating the preparation variables of $LaCoO_3$ with the responses showing good relation between the experimental and predicted values obtained.

The two factors studied in this work, calcination temperature and calcination time, contributed in one way or another, either independently or by combining with each other to influence the three responses with uneven level of contribution. It can clearly be seen from Table 3 that the most significant effect on the removal of both MO and RhB by $LaCoO_3$ was imposed by calcination temperature. This was shown by their highest F-values of 8.36 and 11.81 in comparison with 3.93 and 4.41 imposed by calcination time on MO and RhB removals, respectively. Their interaction effect on MO and RhB removals by $LaCoO_3$ is presented in Fig. 2(a)-(c) as three-

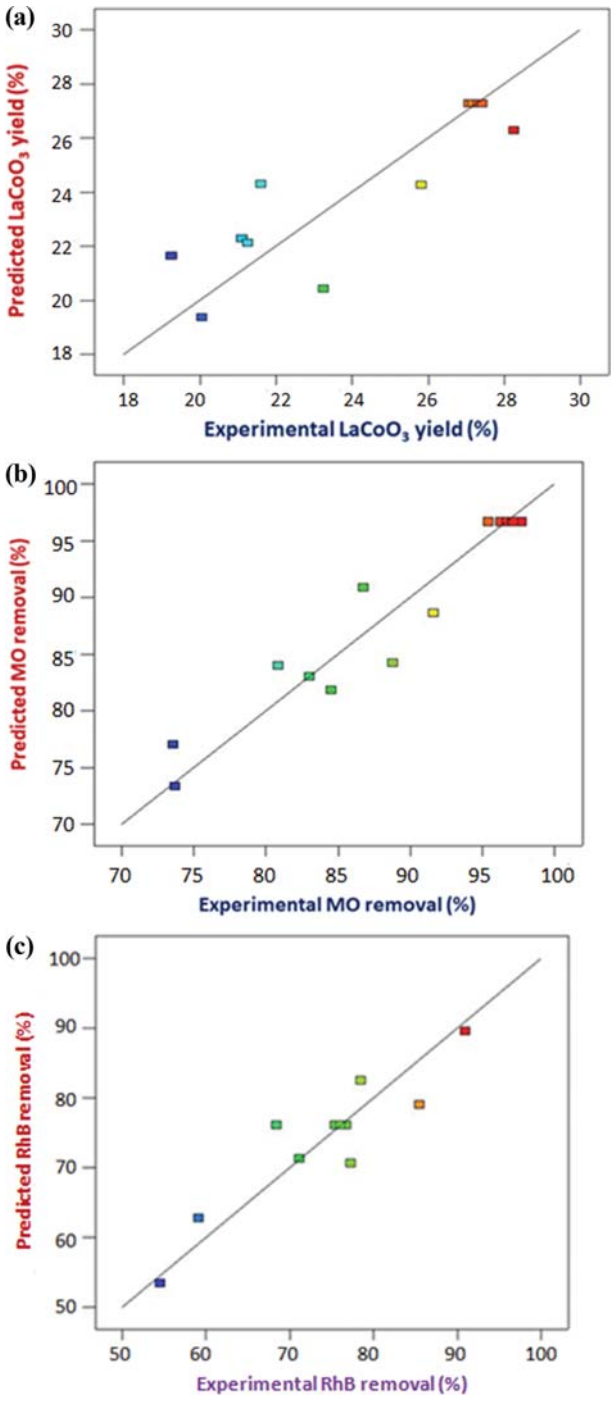

Fig. 1. Relationship between predicted and experimental data for (a) $LaCoO_3$ yield (b) MO removal and (c) RhB removal.

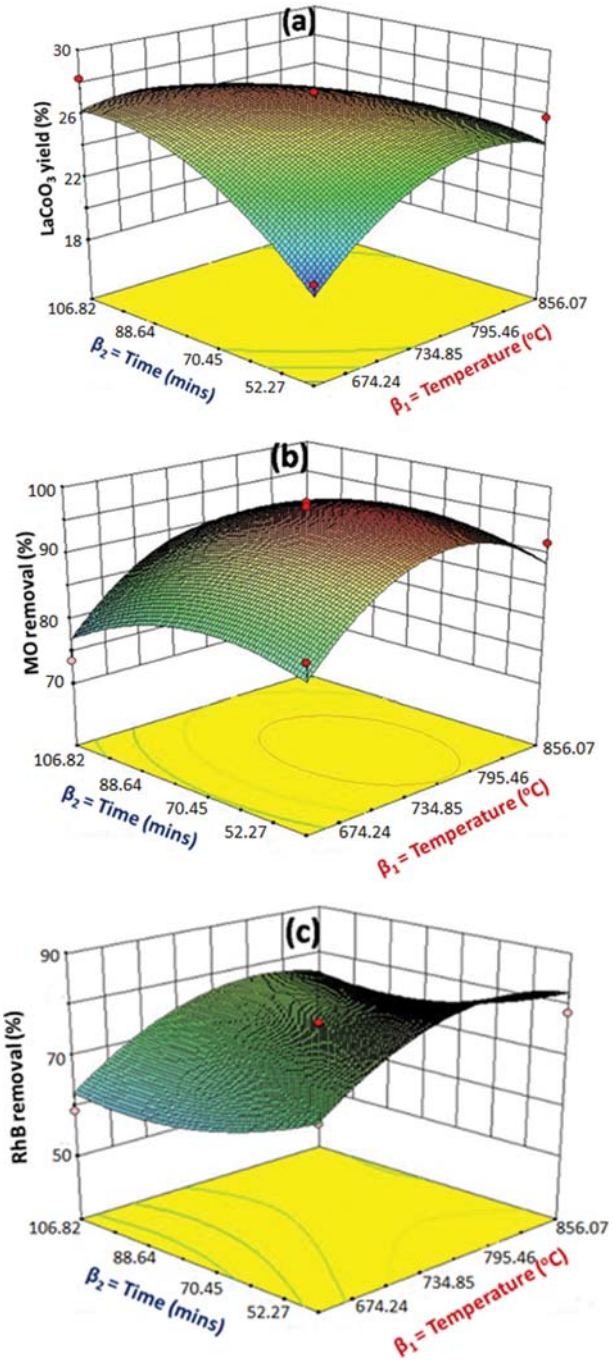

Fig. 2. A three-dimensional (3D) response surface plot showing the effect of calcination temperature and time on (a) $LaCoO_3$ yield (b) MO removal and (c) RhB removal.

dimensional surface figure.

It is not surprising that the optimization result revealed calcination temperature to have an impact on the removal of the dyes because pore and surface area development for adsorbents are enhanced at higher temperatures as reported with respect to other adsorbents [34]. The high percentage removal of MO and RhB by $LaCoO_3$ observed shows a linear relationship with increase in calcination temperature as evident by their quadratic effects in the models revealed. The underwhelming impact imposed by activation time variable on the removal of both MO and RhB was not surprising either, as it has been reported by various researchers in their adsorbent's preparations.

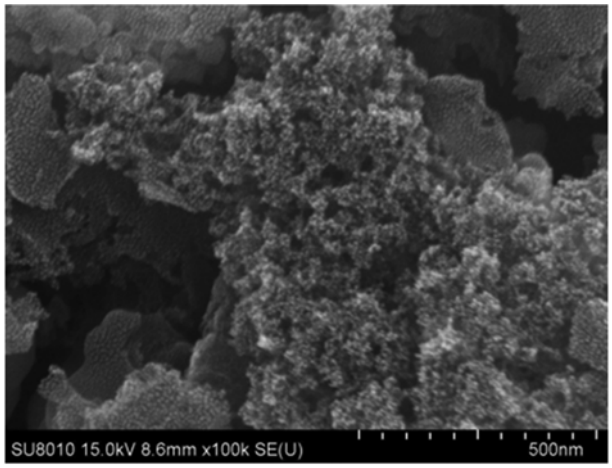

Fig. 3. Scanning electron micrograph (SEM) image of the $LaCoO_3$ adsorbent prepared under optimum conditions (calcination temperature of 775 °C and calcination time of 62 mins).

Activation time was reported by many researchers to have less impact on the increase in pore size and surface area during their adsorbent's preparations [34,39,40], meaning that prolonging activation or calcination time does not necessarily improve the adsorbent surface area, nor does it enlarge the pores on it.

3. Optimization of the Process

This study was aimed at finding the optimum variables that will guide us in preparing an effective $LaCoO_3$ adsorbent capable of removing high percentage of MO and RhB dyes as well as having significant yield. Optimizing these responses under the same conditions is very complicated because the interest regions of factors are poles apart since a dye removal is inversely proportional to the $LaCoO_3$ yield; this prompted us to apply the design-expert software which has the ability to compromise between these responses. The predicted and experimental percentage removal of MO and RhB as well as the adsorbent yield obtained were 97.18; 99.06 and 79.15; 80.94 as well as 26.72; 27.14% which upon comparison lead to error values of 1.55 and 1.90 as well as 2.21%, respectively. The optimum calcination temperature and time obtained for the preparation of $LaCoO_3$ were 775 °C and 62 mins, respectively. The results also revealed that CCD can play a vital role in minimizing cost of producing $LaCoO_3$ composite and at the same time help in avoiding time wastage which can lead to reasonably high yield of adsorbent for its good application in the removal of the two toxic dyes (MO and RhB).

4. Characterization of $LaCoO_3$

The morphology of $LaCoO_3$ was studied by SEM method as shown in Fig. 3. The SEM image of the sample exhibited small and circular particles resembling fine cotton agglomerate. High percentage of the perovskites particles possess a rough looking surface which seems to grow at varying size on the nano scale.

Surface area and porosity are among the most prominent features that indicate a good adsorbent. The BET surface area of $LaCoO_3$ was 61.130 $m^2 g^{-1}$ which compared very well with other adsorbents

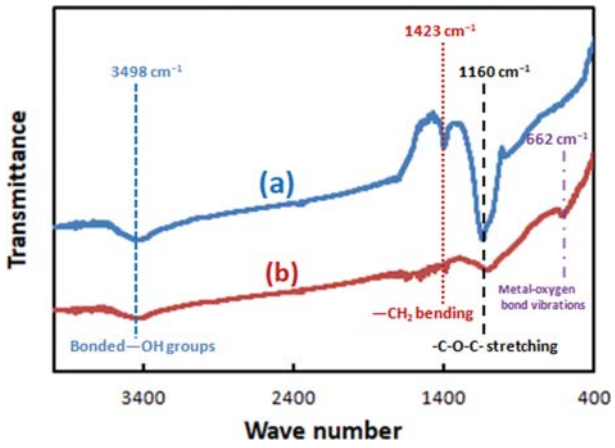

Fig. 4. FTIR spectra of (a) precursor and (b) $LaCoO_3$ perovskite samples.

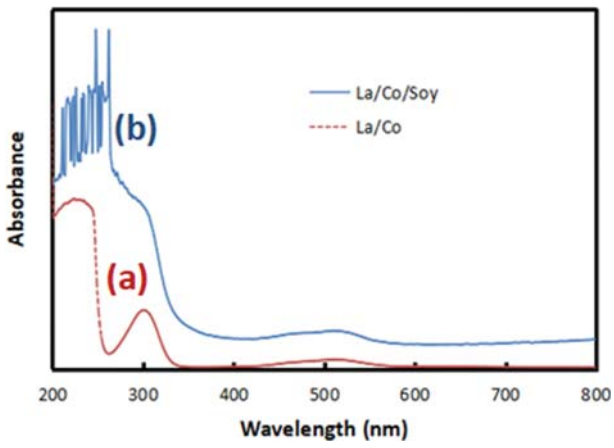

Fig. 5. UV-vis spectra for aqueous system of (a) Co^{2+}/La^{3+} before adding soy protein and (b) Co^{2+}/La^{3+}/soy after addition of soy protein.

such as organoclays (6.036-29.089 $m^2\ g^{-1}$) [41], chitosan/Al_2O_3/magnetite nanoparticles composite (22.070 $m^2\ g^{-1}$) [42], ultrasonic graphene materials (66.720-111.920 m^2/g) [43], hierarchical SnS_2 nanostructure (26.200-48.600 $m^2\ g^{-1}$) [44] and beta zeolites (41-114 $m^2\ g^{-1}$) [45]. The $LaCoO_3$ adsorbent was found to be mesoporous (2-50 nm) with average pore diameter (Dp) of 15.282 nm. The surface area exhibited by the sample, which can be considered high in comparison to literature reports, may be related to the complexing agent used (soy protein) which is formed by amino acids [22,45-47]. The increase in contact surface between reactants was enhanced by fine-powdered soy protein, hence leading to the impregnation of organic matter (in large volumes) into the structure. Thus, the upsurge in surface area as well as pore development during calcination process was enhanced by the elimination of organic materials [48]. Previous studies reported similar behavior which portrayed the increase in the perovskite's surface area by applying polymer treatment as well as engaging a direct reaction with amino acids, which contributed in raising the surface area values from 42 to 59 $m^2\ g^{-1}$ [49].

The observed FTIR spectra in the samples studied (precursor and $LaCoO_3$) are presented in Fig. 4.

From the spectra, there was a broad absorption band at around 3,400-3,500 cm^{-1} which signified the stretching and bending of -OH groups [50]. This may be connected in some way with the interaction between amino acid constituents of soy protein with water. Presence of an asymmetric -CH_2 bending vibration led to the formation of the band at 1,420-1,436 cm^{-1}. This band represents a crystallinity band [51]. Additionally, the peaks in the region of 1,260-1,050 cm^{-1} were assigned to the stretching of C-O in carboxylic acids, alcohols, esters and phenols [30]. It can also be observed from the spectra of $LaCoO_3$ sample (Fig. 4(b)) that the intensity of bands corresponding to organic functional groups reduced significantly after calcination. This was attributed to almost complete disintegration of organic materials present in the samples at 775 °C. A significant band related to the metal-oxygen bond vibrations can also be observed developing on the $LaCoO_3$ spectra at 662 cm^{-1}, which clearly confirmed the interaction between of Co^{2+} and the ligand leading to the formation of the perovskite structure/phase. Similar bands in the same region were reported by [22] for manganese and nickel-based materials as well as [52] for iron-based materials.

The spectrum from UV/visible for the aqueous Co^{2+}/La^{3+} systems prior and after adding soy protein to the system is presented in Fig. 5. A ligand (water) to metal charge-transfer band (LMCT) was attributed to the band observed at 308 nm in the Co^{2+}/La^{3+} spectra [22,53]. Further band at 522 nm can be seen in the system spectrum, which can be allotted to the octahedrally coordinated d-d transitions of Co^{2+}. Those bands are typical of d^8 transition metals in octahedral geometry $^3T_{1g} \leftarrow {}^3A_{2g}$ (P) $^3T_{2g} \leftarrow {}^3A_{2g}$ (F) [54]. Now after the soy protein was introduced as ligand (Co^{2+}/La^{3+}/soy system), the bands at 308 nm were attributed to water still remaining in the system spectrum despite the change of ligand, signifying a contest for coordination with the cation between the two ligands (water and soy protein) [53]. The coordination between the soy protein and Co^{2+} cation was evident based on the presence of ligand to metal charge-transfer band (LMCT) for both systems.

The wavelength of soy protein (260 nm) is lower than 308 nm, making it have higher transition energy, thus becoming a stronger ligand. The soy protein is therefore more preferred to coordinate with the cations bringing inorganic polymer chain into the system, leading to the formation of a more viscous system [53,55].

5. Adsorption Parameters

5-1. Effect of Solution pH

The effect of solution pH on the adsorption of MO and RhB onto $LaCoO_3$ was investigated. The solution pH studied was in the range of 2-12 (Fig. S1(a)). Our results showed a rapid increase in the MO percentage removal from 52.74% to 94.96% with changing pH from 2-4, which was then followed by a small plateau trend in the pH range of 4-10 and then finally decreased by a big margin at pH 12. Similar results were reported from the literature [42,56,57], reporting the optimum pH to be in the range of 3-6 for the MO onto different adsorbents. In our work, the maximum MO removal (94.96%) was observed at the pH of 4. In such case, the only reasonable explanation is the possible occurrence of electrostatic attraction between the $LaCoO_3$ surface (positively charged) and the MO

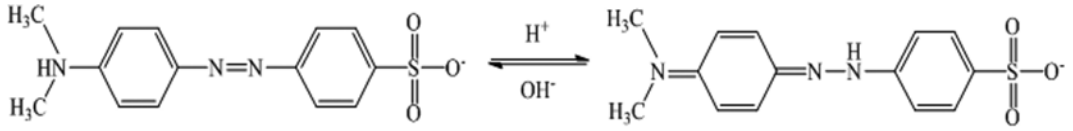

Scheme 1. Rearrangement of MO dye structure from quinoid form (low pH) to azo form (high pH).

dye molecules (negatively charged) as the predominant adsorption mechanism [14].

Another important factor that may influence the adsorption mechanism of the dyes is the pHpzc of the adsorbent and the solution pH by influencing the surface charge as well as causing the disintegration of functional groups over adsorbent surface. We tried to explain the mechanism with respect to the pH_{pzc} value obtained for our $LaCoO_3$ adsorbent, which is 5.8 and MO dye which appeared in quinoid form in acidic solution (low pH). Upon raising the pH to basic condition, it rearranges to azo structure [58] as shown in Scheme 1.

Raising the pH to a value greater than the pH_{pzc} (pH>6) reduces the percentage of MO removed from the solution. We attributed this to the negatively charged perovskite surface ($pH>pH_{pzc}$) causing electrostatic repulsive interaction with the MO as shown from Scheme 1. When pH of the solution is less than the pH_{pzc} value ($pH<pH_{pzc}$), the surface then has a net positive charge which draws the anionic MO dye molecule to it due to electrostatic attraction between anionic dye molecule and positively charged $LaCoO_3$ surface.

With respect to RhB, it can be seen that raising the solution pH from 4 to 12 leads to a drastic fall in RhB removal values from 80.42 to 47.87% (Fig. S1(a)). Similar observation was reported by other researchers [59-61] using different adsorbents. Similar reason as explained in the case of MO removal is also thought to be behind RhB adsorption at lower pH. Maurya and co-researchers also explained the reason behind RhB removal at low pH based on their adsorbent's pH_{pzc} value [62]. They reported their adsorbent's surface to be positively charged at $pH<pH_{pzc}$ (4.05), thus prompting the surface to have affinity for the ionic form of RhB dye, which promoted enhanced adsorption at low pH [62]. The availability of some carboxylic anions on the dye in the solution is another reason attributed to the RhB removal at low pH, which influences the positively charged adsorbent surface to be the preferred site for the adsorption process to take place [63]. This therefore helped us in choosing pH 4 as the optimum pH for further experiments on MO and RhB removals.

5-2. Effect of Contact Time

For the sake of optimizing the equilibration time, the adsorption of MO and RhB on $LaCoO_3$ was also studied at varying contact time (Fig. S1(b)). At the initial stage, MO and RhB dyes' uptake was observed to be very fast as observed at the initial stage, suggesting an external adsorption on the surface. Internal surface adsorption was more pronounced at the final phase, which was relatively slower [56]. Different equilibrium times were established with respect to the adsorption of RhB and MO at the same concentration fixed at 100 mg L^{-1} which were around 150 and 400 mins, respectively. Rapid adsorption with respect to both dyes can be seen to have taken place on the external surface of the adsorbent at initial stage, which was then followed by slower internal diffusion process (the rate determining step) attributed to the fact that at this stage, a large number of surface sites are occupied from the initial stage and therefore unavailable for adsorption because of the repulsion between the bulk phases and solute molecules [64].

5-3. Effect of Adsorbent Dosage

To get the optimum amount of the adsorbent required for the effective adsorption of the MO and RhB molecules, varying doses of $LaCoO_3$ (200-1,000 mg) were added to both the MO and RhB solutions and shaken for the respective equilibrium times with the results presented in Fig. S1(c). With respect to MO, the result demonstrated an increase in the removal efficiency from 93.21% to 95.07% after increasing the $LaCoO_3$ dosage from 100 to 200 mg, which was then followed by a plateau trend upon further increment in the adsorbent dose with no significant increase in the MO removal beyond the concentration of 300 mg; hence, further increase of adsorbent dosage did not enhance the removal percentage. On the other hand, the percentage adsorption of RhB at equilibrium was directly proportional to increasing dosages of $LaCoO_3$ (Fig. S1(c)). At dosage above 500 mg, the percentage removal of Rhd B slightly decreased. This was attributed to the maximum adsorption capacity being reached as well as the number of free dye molecules and that of the RhB molecules bound to the adsorbent and remaining constant even with a greater dose of the adsorbent [65].

6. Theoretical Evaluation of Equilibrium and Kinetic Data

Langmuir, Freundlich, Temkin, Sips and Toth isotherm equations were plotted to dissect the equilibrium data and determine the best-fitted model for the adsorption of both MO and RhB with the respective plots depicted in Fig. S2(a)-(e). Theoretical parameters from the isotherms (Q_a^0, K_L, R_L, K_β, n, A, B, b_S, n_p, K_t) and the correlation coefficients (R^2) obtained from those plots are compiled in Table 4. The maximum adsorption capacity (Q_a^0) values for MO and RhB removal by $LaCoO_3$ were observed to decrease with an increase in temperature, suggesting the adsorption process with respect to both dyes to be exothermic. Putting into consideration the environmentally friendly design aspect, $LaCoO_3$ can be said to be a promising adsorbent material for MO and RhB in wastewater based on the maximum adsorption capacity values.

Additionally from Table 4, all the R_L values reported for MO and RhB at all temperatures are between 0 and 1, confirming favorable adsorption under the studied conditions. Meanwhile, n values for both MO and RhB depicted from the Freundlich isotherm model are greater than unity, confirming the suitability of $LaCoO_3$ as good adsorbent for the removal of both dyes. The values of A and B were also evaluated from the Temkin model. Still from the fitting results listed in Table 4, the Freundlich isotherm model with the highest R^2 values appeared to be much more applicable in the adsorption of both MO and RhB dyes, meaning that the dye molecules from bulk solution were adsorbed on heterogeneous surface. Both of the three-parameter isotherms (Sips and Toth) also

Table 4. Langmuir, Freundlich, Temkin, Sips and Toth isotherm models for MO and RhB adsorption onto $LaCoO_3$ at different temperatures

Isotherms	Parameters	MO			RhB		
		30 °C	40 °C	50 °C	30 °C	40 °C	50 °C
Langmuir	Q_a^0 (mg g^{-1})	223.55	211.93	204.82	238.95	235.81	229.67
	K_L (L mg^{-1})	0.074	0.057	0.045	0.018	0.016	0.014
	R_L	0.051	0.066	0.082	0.182	0.0.200	0.222
	R^2	0.9776	0.9611	0.9394	0.9627	0.9693	0.9221
	χ^2	0.169	0.178	0.150	0.060	0.017	0.041
Freundlich	K_F (mg^{1-n} g^{-1} L^n)	26.908	22.837	18.788	8.103	7.387	6.443
	n	2.070	2.077	1.999	1.521	1.508	1.489
	R^2	0.9958	0.9994	0.9928	0.9874	0.9899	0.9808
	χ^2	0.009	0.001	0.014	0.025	0.002	0.039
Temkin	A (L/g)	0.002	0.902	0.649	0.234	0.214	0.189
	B (J/mol)	40.243	38.216	38.295	45.862	44.913	43.624
	R^2	0.9444	0.9346	0.9289	0.9548	0.9560	0.9415
	χ^2	1.964	1.552	0.216	0.171	0.172	0.153
Sips	1/n	0.817	0.786	0.798	1.0917	1.109	1.076
	b_S (L g^{-1})	0.090	0.068	0.053	0.038	0.034	0.029
	R^2	0.9765	0.9889	0.9997	0.9993	0.9995	0.9941
	χ^2	2.394	1.245	1.716	3.711	3.712	2.513
Toth	n_t	0.896	0.879	0.886	1.053	1.064	1.043
	K_t	0.065	0.045	0.036	0.040	0.039	0.032
	R^2	0.9809	09924	0.9997	0.9994	0.9994	0.9948
	χ^2	5.400	4.892	3.601	5.001	3.783	4.893

Table 5. Adsorption capacity of different adsorbents for MO and RhB dyes removal at 30 °C

Adsorbent	Adsorbate	Q_a^0 (mg g^{-1})	Reference
$LaCoO_3$	MO	223.55	This work
Immobilized polyaniline	MO	77.3	[66]
POCa porous microsphere	MO	35.21	[67]
Ammonium-functionalized silica nanoparticle	MO	105.4	[68]
Fabricated chitosan microspheres	MO	207	[69]
Synthesized hierarchical SnS_2 nanostructure	RhB	200	[44]
Poly(lactic acid)/activated carbon composite bead	RhB	149.57	[70]
Beta zeolites	RhB	29.97	[45]
$LaCoO_3$	RhB	238.95	This work

show good fit based on the R^2 values obtained as shown in Table 4.

To further confirm the selection of best fitted model for the experimental data, chi square (χ^2) was incorporated since correlation coefficient (R^2) may not be reliable enough in justifying the basis for selection of the best adsorption model, because it only represents the fit between experimental data and linearized forms of the isotherm equations, while chi square (χ^2) represents the fit between the experimental and predicted values of the adsorption capacity. The lower the χ^2 value, the better the fit. So still from Table 4, the Freundlich model can be seen to show the least magnitude of χ^2 as well as R^2 values closest to unity at all temperatures, which further confirms it as the best isotherm model in describing the adsorption processes. Other researchers reported similar observation [32].

The maximum adsorption capacity of $LaCoO_3$ was compared with a selection of other adsorbents (Table 5). The data from Table 5 clearly confirm the effectiveness of $LaCoO_3$ adsorbent in the removal of MO and RhB dyes from the aqueous solution.

For more insight into the nature of MO and RhB adsorption onto $LaCoO_3$, the adsorption kinetics data generated were fitted by the pseudo-first-order, pseudo-second-order and intra-particle diffusion kinetic models [71,72] with their respective equations respectively expressed as:

$$\log(q_e - q_t) = \log q_e - \frac{k_1}{2.303}t \quad (15)$$

$$\frac{t}{q_t} = \frac{1}{k_2 q_e^2} + \frac{1}{q_e}t \quad (16)$$

Table 6. Kinetic models parameters for the adsorption of MO and RhB onto $LaCoO_3$ at 30 °C

Parameter	Pseudo-first order model				Pseudo-second order model			Intra-particle diffusion model		
	$q_{e\,exp}$ (mg g^{-1})	k_1 (min^{-1})	$q_{e\,cal}$ (mg g^{-1})	R^2	$k_2\times10^{-5}$ (g mg^{-1} h)	$q_{e\,cal}$ (mg g^{-1})	R^2	k_p (mg g^{-1} $h^{0.5}$)	C	R^2
MO	188	0.010	170.373	0.9962	5.207	232.558	0.9976	11.200	4.234	0.9487
RhB	153.1	0.013	84.625	0.8182	16.458	172.414	0.9932	12.548	2.843	0.9744

$$q_t = k_{pi} t^{0.5} + C \quad (17)$$

where q_e and q_t are the amounts adsorbed (mg g^{-1}) at equilibrium and at time t (h), respectively, while k_1 (h^{-1}) and k_2 (g mg^{-1} h) are the adsorption rate constants of pseudo first and second-order adsorption, respectively, k_{pi} is rate constant of the intra-particle diffusion equation, and C gives information about the boundary layer thickness: A larger value of C is associated with the boundary layer diffusion effect.

Fig. S3(a)-(c) shows the fitting curves for the models from where the kinetic parameters presented in Table 6 were evaluated.

The R^2 values for pseudo-first-order model (Fig. S3(a)) and the intra-particle diffusion (Fig. S3(c)) were smaller when compared with the values obtained from pseudo-second-order model (Fig. S3(b)) with respect to both MO and RhB dyes (Table 6), confirming pseudo-second-order model to be the best fit with respect to both MO and RhB adsorptions onto $LaCoO_3$ adsorbent. Additionally, the linear lines of the intraparticle plots (Fig. S3(c)) for both MO and RhB dyes have an intercept not equal to zero, signifying that other rate controlling steps are involved in the process in addition to the intraparticle diffusion.

7. Adsorption Thermodynamic Parameters

The standard Gibb's free energy change (ΔG^o), enthalpy (ΔH^o) and entropy (ΔS^o) were the thermodynamic parameters evaluated to give an idea about the feasibility and spontaneity of the adsorption process. Van't Hoff equation was employed in computing the thermodynamic parameters

$$\ln K_L^o = \frac{\Delta S^o}{R} - \frac{\Delta H^o}{RT} \quad (18)$$

whereby R is the universal gas constant of 8.314 J mol^{-1} K^{-1}, T is the temperature (K), and K_L^o is the (dimensionless) 'thermodynamic' Langmuir constant for the adsorption process. To obtain K_L^o, the value of K_L (L mg^{-1}) extrapolated from the Langmuir isotherm plot (Eq. (4)) was used as expressed below [73].

$$K_L^o = K_L\ (\text{L mg}^{-1}) \times 1000\ (\text{mg g}^{-1}) \times \text{Mwt of dye}\ (\text{g mol}^{-1}) \times C^o\ (\text{mol L}^{-1}) \quad (19)$$

All the concentrations were changed to molar form in order to take into account the standard state, C^o=1 mol L^{-1} [73], Mwt of dye= molecular weight of the MO (327.33 g mol^{-1}) and RhB (479.02 g mol^{-1}) dyes, 1000 is a conversion factor from gram (g) to milligram (mg). A linear plot of $\ln K_L^o$ against 1/T gives a graph by which ΔH^o and ΔS^o were obtained from the slope and intercept, respectively. The adsorption process is referred to as spontaneous and exothermic if ΔG^o and ΔH^o are less than 0, respectively. Furthermore, if $\Delta H^o > T\Delta S^o$, the adsorption process is enthalpy driven; otherwise, it is an entropy driven process. [27]. ΔG^o was calculated using Eq. (20):

Table 7. Thermodynamic parameters for the adsorption of MO and RhB onto $LaCoO_3$ at different temperatures

Dyes	T(K)	ΔH^o (kJ mol^{-1})	ΔS^o (J mol^{-1} K)	ΔG^o (kJ mol^{-1})
MO	303	−3.35	6.38	−25.43
	313			−25.59
	323			−25.77
RhB	303	−6.60	3.25	−22.83
	313			−22.53
	323			−23.66

$$\Delta G^o = -RT \ln K_L^o \quad (20)$$

The adsorption of both MO and RhB dyes onto $LaCoO_3$ shows negative ΔH^o values (Table 7), implying that the adsorption processes were exothermic, which agreed with results from Table 4. In an exothermic adsorption process, the difference between energy released and energy absorbed during the bond making and breaking between the dyes and adsorbent gave rise to the energy released in form of heat [74]. The result also suggests a high tendency of decrease in solubility of both MO and RhB in solution at higher temperature, making them more difficult to be adsorbed [75]. It has further been reported that ΔH^o value less than 40 kJ mol^{-1} signifies physisorption [76]; therefore, the values obtained with respect to both dyes imply that the adsorption is a physisorption process.

The Gibb's free energy of change (ΔG^o) for the adsorption of both dyes shows negative values (Table 7). The values obtained with respect to both MO and RhB dyes signified feasible and spontaneous process for both dyes with the similarity in the values, indicating that such spontaneous adsorption is independent of the temperature.

The entropy (ΔS^o) values obtained for the adsorption of both MO and RhB dyes were positive, as can be seen in Table 4. This implies an inclination between the adsorbates and adsorbent. Another explanation is the occurrence of structural changes in the adsorbent and the dyes due to increase in randomness at an interface comprising the adsorbent/dye solution as well as an increase in the degree of freedom. Other researchers suggested an increase in the degree of freedom in the adsorption system to be related to the much translational entropy gained by adsorbed solvent molecules than was lost by the dye molecules [77]. Other researchers reported a similar observation [78].

8. Regeneration of the Used Adsorbent

The reusability of $LaCoO_3$ adsorbent is an important parameter considered in this work due to its economic importance, especially that the work was carried out within the framework of a sustainable development approach, which led to our decision of

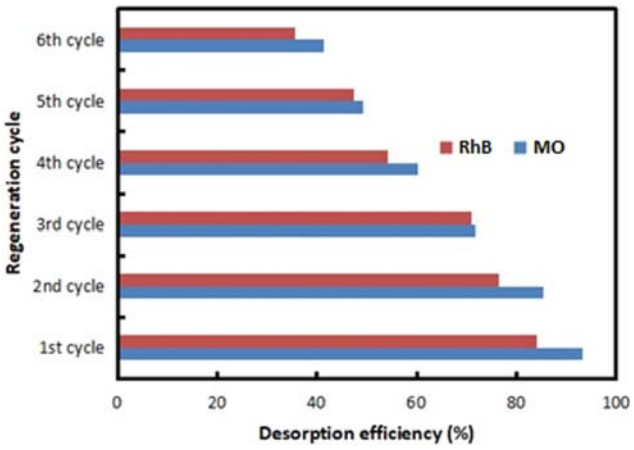

Fig. 6. Reusability of the $LaCoO_3$ perovskite adsorbent in the removal of MO and RhB.

limiting our desorption studies to using only one solvent reported from literature as the best and most effective eluent. Fig. 6 shows the result of our regeneration analysis revealing that $LaCoO_3$ could be used about six times before being disposed after the efficiency came down to less than 40%. This behavior signified that the adsorbent can successfully hold on to the two dyes after their adsorption from aqueous solution. This is related to the porosity and surface area of the adsorbent as determined through characterization [79]. The electrostatic repulsion which occurred upon changes in the solution chemistry was reported to be responsible for the feasibility of desorption of the adsorbed MO and RhB dye molecules on the adsorbent with similar observation reported by other researchers [80]. Our regeneration results also further prove the literature report of ethanol desorption technique being the propitious way of regenerating spent adsorbents having good reusability [36,81].

9. Adsorption Mechanism

As reported earlier (sub-section 3.5.1), the adsorption mechanism of the dyes may be influenced by the pH_{pzc} of the adsorbent as well as the solution pH suggesting electrostatic attraction between the positively charged $LaCoO_3$ surface and anionic MO dye molecule. Aside from electrostatic interactions, hydrogen bonding interaction and hydrophobic interactions (π-π stacking) [61,82,83] may possibly occur between MO, RhB and the surface of $LaCoO_3$. The possibility of hydrogen bonding interaction could be between the hydroxyl group from water in the solution and the oxygen atoms present on the dye molecules [61]. It may also occur between all of N, OH, O atoms in MO and RhB dye molecules with the hydroxyl group from the adsorbed H_2O on surface of metal ions of $LaCoO_3$ perovskite. At lower pH, there is also the possibility of hydrophobic interactions (π-π stacking) to occur between the aromatic rings of MO and RhB and the $LaCoO_3$ surface. Additionally, as reported by other researchers, the positive charge of RhB^+ plays a big role in enhancing the π-π stacking interactions [82]. The proposed adsorption mechanism of MO and RhB molecules onto the surface of $LaCoO_3$ is depicted in Scheme 2.

CONCLUSIONS

A facile, modified proteic method using soy protein (complexing agent) can be used efficiently to synthesize $LaCoO_3$ perovskite nanoparticles as an effective adsorbent. The perovskite material in our work was prepared at optimum calcination temperature and time of 775 °C and 62 mins, respectively, which were determined with the aid of CCD statistical technique. The parameters optimized by the software gave rise to the predicted and experimental percentage removals of MO and RhB as well as the adsorbent yield of 97.18; 99.06 and 79.15; 80.94 as well as 26.72; 27.14%, which upon comparison led to error values of 1.55 and 1.90 as well as 2.21%, respectively. The equilibrium and kinetics of the adsorption process with respect to MO and RhB on the $LaCoO_3$ perovskite material were best described by Langmuir and Freundlich isotherms as well as pseudo-second-order kinetic models, respec-

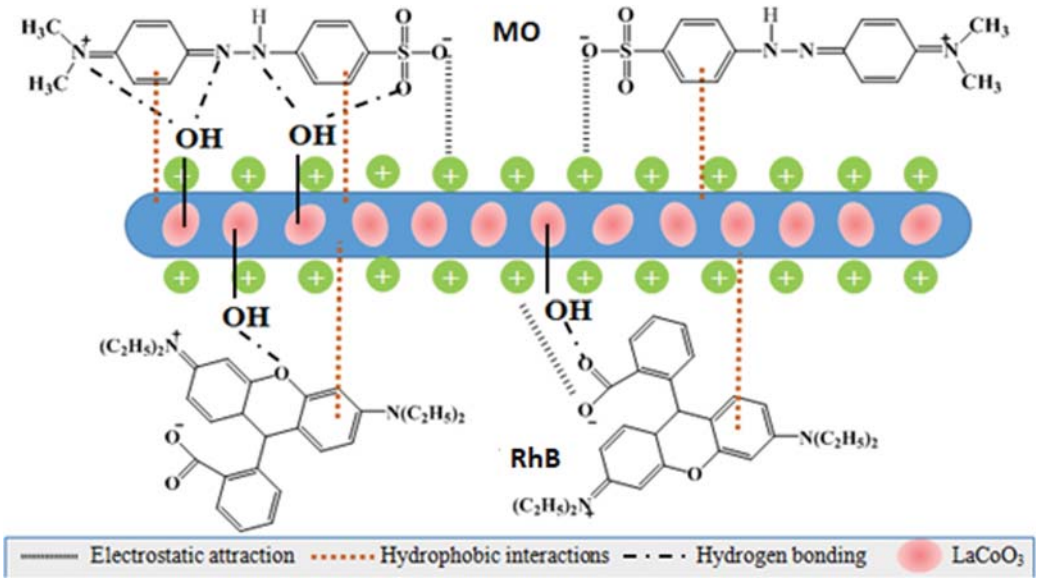

Scheme 2. Possible adsorption mechanism of MO and RhB dyes on $LaCoO_3$.

tively. Textural characterization shows the $LaCoO_3$ to have a BET surface area, total pore volume and average pore diameter of 61.130 $m^2 g^{-1}$, 0.125 $cm^3 g^{-1}$ and 15.282 nm, respectively. The optimization analysis successfully revealed that $LaCoO_3$ perovskite material with high yield and good removal of MO and RhB can be synthesized by modified proteic method, which compared very well with some conventional adsorbents and should be further evaluated in the elimination of other organic molecules such as drugs.

ACKNOWLEDGEMENTS

The authors humbly acknowledge the international funding provided by Fujian Agriculture and Forestry University (KXB16001A) and the Department of Science and Technology of Fujian Province (2017H6003), P.R. China.

CONFLICT OF INTEREST

The authors have no conflict of interest with regards to the submission and publication of this article.

SUPPORTING INFORMATION

Additional information as noted in the text. This information is available via the Internet at http://www.springer.com/chemistry/journal/11814.

REFERENCES

1. M. E. Argun, D. Güclü and M. Karatas, *J. Ind. Eng. Chem.*, **20**, 1079 (2014).
2. M. Shaban, M. R. Abukhadra, A. A. Parwaz Khan and B. M. Jibali, *J. Taiwan Inst. Chem. Eng.*, **82**, 102 (2018).
3. F. Banat, S. Al-Asheh, R. Al-Ahmad and F. Bni-Khalid, *Bioresour. Technol.*, **98**, 3017 (2007).
4. G. Crini, *Bioresour. Technol.*, **97**, 1061 (2006).
5. E. Brillas and C. A. Martínez-Huitle, *Appl. Catal. B*, **166-167**, 603 (2015).
6. V. Khandegar and A. K. Saroha, *J. Environ. Manage.*, **128**, 949 (2013).
7. M. Bradha, T. Vijayaraghavan, S. P. Suriyaraj, R. Selvakumar and A. M. Ashok, *J. Rare Earths*, **33**, 160 (2015).
8. T. Santhi, A. L. Prasad and S. Manonmani, *Arab. J. Chem.*, **7**, 494 (2014).
9. Y.-D. Chen, W.-Q. Chen, B. Huang and M.-J. Huang, *Chem. Eng. Res. Des.*, **91**, 1783 (2013).
10. M. H. Dehghani, A. Zarei, A. Mesdaghinia, R. Nabizadeh, M. Alimohammadi, M. Afsharnia and G. McKay, *Chem. Eng. Res. Des.*, **140**, 102 (2018).
11. Z. N. Garba, F. B. S. Shikin and A. R. Afidah, *J. Chem. Eng. Chem. Res.*, **2**, 623 (2015).
12. Z. N. Garba, A. R. Afidah and B. Z. Bello, *J. Environ. Chem. Eng.*, **3**, 2892 (2015).
13. H. Tavakkoli and M. Yazdanbakhsh, *Micropor. Mesopor. Mater.*, **176**, 86 (2013).
14. M. Yazdanbakhsh, H. Tavakkoli and S. M. Hosseini, *Desalination*, **281**, 388 (2011).
15. M. Algueró, P. Ramos, R. Jiménez, H. Amorín, E. Vila and A. Castro, *Acta Mater.*, **60**, 1174 (2012).
16. C. Moure and O. Peña, *Solid State Chem.*, **43**, 148 (2015).
17. R. G. Shetkar and A. V. Salker, *J. Mater. Sci. Technol.*, **26**, 1098 (2010).
18. R. Guo, T. Jiao, R. Li, Y. Chen, W. Guo, L. Zhang, J. Zhou, Q. Zhang and Q. Peng, *ACS Sustainable Chem. Eng.*, **6**, 1279 (2018).
19. K. Li, T. Jiao, R. Xing, G. Zou, J. Zhou, L. Zhang and Q. Peng, *Sci. China Mater.*, **61**, 728 (2018).
20. R. Guo, R. Wang, J. Yin, T. Jiao, H. Huang, X. Zhao, L. Zhang, Q. Li, J. Zhou and Q. Peng, *Nanomater.*, **9**, 127 (2019).
21. X. Huang, R. Wang, T. Jiao, G. Zou, F. Zhan, J. Yin, L. Zhang, J. Zhou and Q. Peng, *ACS Omega*, **4**, 1897 (2019).
22. A. G. Santos, J. O. Leite, M. J. B. Souza, I. F. Gimenez and A. M. Garrido Pedrosa, *Ceram. Int.*, **44**, 5743 (2018).
23. E. Grabowska, *Appl. Catal. B*, **186**, 97 (2016).
24. Z. N. Garba and A. R. Afidah, *J. Anal. Appl. Pyrol.*, **107**, 306 (2014).
25. J. Nsor-Atindana, M. Chen, H. D. Goff, F. Zhong, H. R. Sharif and Y. Li, *Carbohyd. Polym.*, **172**, 159 (2017).
26. G. Thoorens, F. Krier, B. Leclercq, B. Carlin and B. Evrard, *Int. J. Pharm.*, **473**, 64 (2014).
27. X. Zhang, Y. Wu, X. Li, X. Meng, H. Shi, Z. Wu and J. Zhang, *Korean J. Chem. Eng.*, **36**, 753 (2019).
28. Z. N. Garba, A. R. Afidah and S. A. Hamza, *J. Environ. Chem. Eng.*, **2**, 1423 (2014).
29. M. A. Ahmad and R. Alrozi, *Chem. Eng. J.*, **165**, 883 (2010).
30. C. W. Oo, M. J. Kassim and A. Pizzi, *Ind. Crop. Prod.*, **30**, 152 (2009).
31. W. S. Wan Ngah, S. Fatinathan and N. A. Yosop, *Desalination*, **272**, 293 (2011).
32. L. T. Popoola, A. S. Yusuff, O. A. Adesina and M. A. Lala, *J. Environ. Sci. Technol.*, **12**, 65 (2019).
33. R. Baccar, P. Blánquez, J. Bouzid, M. Feki, H. Attiya and M. Sarrà, *Fuel Proces. Technol.*, **106**, 408 (2013).
34. M. Auta and B. H. Hameed, *Chem. Eng. J.*, **175**, 233 (2011).
35. H. Deng, L. Yang, G. Tao and J. Dai, *J. Hazard. Mater.*, **166**, 1514 (2009).
36. S. Deng, Y. Nie, Z. Du, Q. Huang, P. Meng, B. Wang, J. Huang and G. Yu, *J. Hazard. Mater.*, **282**, 150 (2015).
37. J. N. Sahu, J. Acharya and B. C. Meikap, *Bioresour. Technol.*, **101**, 1974 (2010).
38. M. A. Ahmad and R. Alrozi, *Chem. Eng. J.*, **171**, 510 (2010).
39. M. K. B. Gratuito, T. Panyathanmaporn, R. A. Chumnanklang, N. Sirinuntawittaya and A. Dutta, *Bioresour. Technol.*, **99**, 4887 (2008).
40. Ç. D. Şentorun-Shalaby, M. G. Uçak-Astarlıogˇlu, L. Artok and Ç. Sarıcı, *Micropor. Mesopor. Mater.*, **88**, 126 (2006).
41. L. Zhang, B. Zhang, T. Wu, D. Sun and Y. Li, *Colloids Surf., A: Physicochem. Eng. Aspects*, **484**, 118 (2015).
42. B. Tanhaei, A. Ayati, M. Lahtinen and M. Sillanpää, *Chem. Eng. J.*, **259**, 1 (2015).
43. T. Soltani and B.-K. Lee, *J. Colloid Interface Sci.*, **481**, 168 (2016).
44. S. Wang, B. Yang and Y. Liu, *J. Colloid Interface Sci.*, **507**, 225 (2017).
45. Z.-L. Cheng, Y.-X. Li and Z. Liu, *Ecotoxicol. Environ. Safety*, **148**, 585 (2018).
46. Y. Ma, X. Y. Wu and G. K. Zhang, *Appl. Catal. B,-Environ.*, **205**, 262 (2017).
47. J. C. Santos, M. J. B. Souza, M. E. Mesquita and A. M. G. Pedrosa,

Sci. Plen., Sci. Plen., **8**, 1 (2012).
48. G. Leofanti, M. Padovan, G. Tozzola and B. Venturelli, *Catal. Today*, **41**, 207 (1998).
49. A. G. Margellou, I. T. Papadas, D. E. Petrakis and G. S. Armatas, *Mater. Res. Bull.*, **83**, 491 (2016).
50. Q. Q. Shi, J. Zhang, C. L. Zhang, C. Li, B. Zhang, W. W. Hu and J. T. Xu, *J. Environ. Sci.*, **22**, 91 (2010).
51. C. H. C. Tan, S. Sabar and M. H. Hussin, *South African J. Chem. Eng.*, **26**, 11 (2018).
52. A. Benaicha and M. Omari, *J. Fundam. Appl. Sci.*, **10**, 132 (2018).
53. P. W. Atkins, T. L. Overton, J. P. Rourke and M. T. Weller, Shriver and Atkins' W. H. Freeman and Company, 5th Ed. New York (2010).
54. J. C. Santos, M. J. B. Souza, J. A. C. Ruiz, D. M. A. Melo, M. E. Mesquita and A. M. G. Pedrosa, *J. Braz. Chem. Soc.*, **23**, 1858 (2012).
55. C. J. Jones, Bookman, Porto Alegre, RS (2002).
56. S. Hosseini, M. A. Khan, M. R. Malekbala, W. Cheah and T. S. Y. Choong, *Chem. Eng. J.*, **171**, 1124 (2011).
57. R. Huang, Q. Liu, J. Huo and B. Yang, *Arab. J. Chem.*, **10**, 24 (2017).
58. H. Z. Ma, B. Wang and X. Y. Luo, *J. Hazard. Mater.*, **149**, 492 (2007).
59. S. Khamparia and D. Jaspal, *J. Environ. Manage.*, **183**, 786 (2016).
60. P. K. Satapathy, M. Das and A. K. Sahoo, *Indian J. Chem. Technol.*, **21**, 257 (2014).
61. M. Mohammadi, A. J. Hassani, A. R. Mohamed and G. D. Najafpour, *J. Chem. Eng. Data*, **55**, 5777 (2010).
62. N. S. Maurya, A. K. Mittal, P. Cornel and E. Rother, *Bioresour. Technol.*, **97**, 512 (2006).
63. T. Soltani and M. H. Entezari, *Chem. Eng. J.*, **223**, 145 (2013).
64. B. H. Hameed and M. I. El-Khaiary, *J. Hazard. Mater.*, **159**, 574 (2008).
65. F. Hayeeye, M. Sattar, W. Chinpa and O. Sirichote, *Colloids Surf., A: Physicochem. Eng. Aspects*, **513**, 259 (2017).
66. N. N. Bahrudin, M. A. Nawi and W. I. N. W. Ismail, *Korean J. Chem. Eng.*, **35**, 1450 (2018).
67. M. N. Anjum, K. M. Zia, L. Zhu, Haroon-ur-Rashid, M. N. Ahmad, M. Zuber and H. Tang, *Korean J. Chem. Eng.*, **31**, 2192 (2014).
68. J. Liu, S. Ma and L. Zang, *Appl. Surf. Sci.*, **265**, 393 (2013).
69. L. Zhai, Z. Bai, Y. Zhu, B. Wang and W. Luo, *Chinese J. Chem. Eng.*, **26**, 657 (2018).
70. M. Sattar, F. Hayeeye, W. Chinpa and O. Sirichote, *J. Environ. Chem. Eng.*, **5**, 3780 (2017).
71. L. Largitte and R. Pasquier, *Chem. Eng. Res. Des.*, **112**, 289 (2016).
72. L. Largitte and R. Pasquier, *Chem. Eng. Res. Des.*, **109**, 495 (2016).
73. L. Mouni, L. Belkhiri, J.-C. Bollinger, A. Bouzaza, A. Assadi, A. Tirri, F. Dahmoune, K. Madani and H. Remini, *Appl. Clay Sci.*, **153**, 38 (2018).
74. P. Saha and S. Chowdhury, *Intech*, **16**, 349 (2011).
75. D. Duranoğlu, A. W. Trochimczuk and U. Beker, *Chem. Eng. J.*, **187**, 193 (2012).
76. S. Jiancheng, L. Renlong, W. Haiping, L. Zuohua, S. Xiaolong and T. Changyuan, *J. Taiwan Inst. Chem. Eng.*, **82**, 351 (2018).
77. G. Z. Kyzas, N. K. Lazaridis and A. C. Mitropoulos, *Chem. Eng. J.*, **189-190**, 148 (2012).
78. P. Liao, Z. Malik Ismael, W. Zhang, S. Yuan, M. Tong, K. Wang and J. Bao, *Chem. Eng. J.*, **195-196**, 339 (2012).
79. O. Hernandez-Ramirez and S. M. Holmes, *J. Mater. Chem.*, **18**, 2751 (2008).
80. N. M. Mahmoodi, B. Hayati, M. Arami and C. Lan, *Desalination*, **268**, 117 (2011).
81. I. A. W. Tan, A. L. Ahmad and B. H. Hameed, *J. Hazar. Mater.*, **164**, 473 (2009).
82. Y. Qiu, Z. Zheng, Z. Zhou and G. D. Sheng, *Bioresour. Technol.*, **100**, 5348 (2009).
83. Y. Yu, B. N. Murthy, J. G. Shapter, K. T. Constantopoulos, N. H. Voelcker and A. V. Ellis, *J. Hazard. Mater.*, **260**, 330 (2013).

Supporting Information

Process optimization and synthesis of lanthanum-cobalt perovskite type nanoparticles ($LaCoO_3$) prepared by modified proteic method: Application of response surface methodology

Zaharaddeen N. Garba[*,], Wei Xiao[*], Weiming Zhou[*], Ibrahim Lawan[*], Yifan Jiang[*], Mingxi Zhang[*], and Zhanhui Yuan[*,†]**

*College of Materials Science and Engineering, Fujian Agriculture and Forestry University, Fuzhou, Fujian Province, China
**Department of Chemistry, Ahmadu Bello University Zaria, Nigeria
(*Received 5 July 2019 • accepted 8 October 2019*)

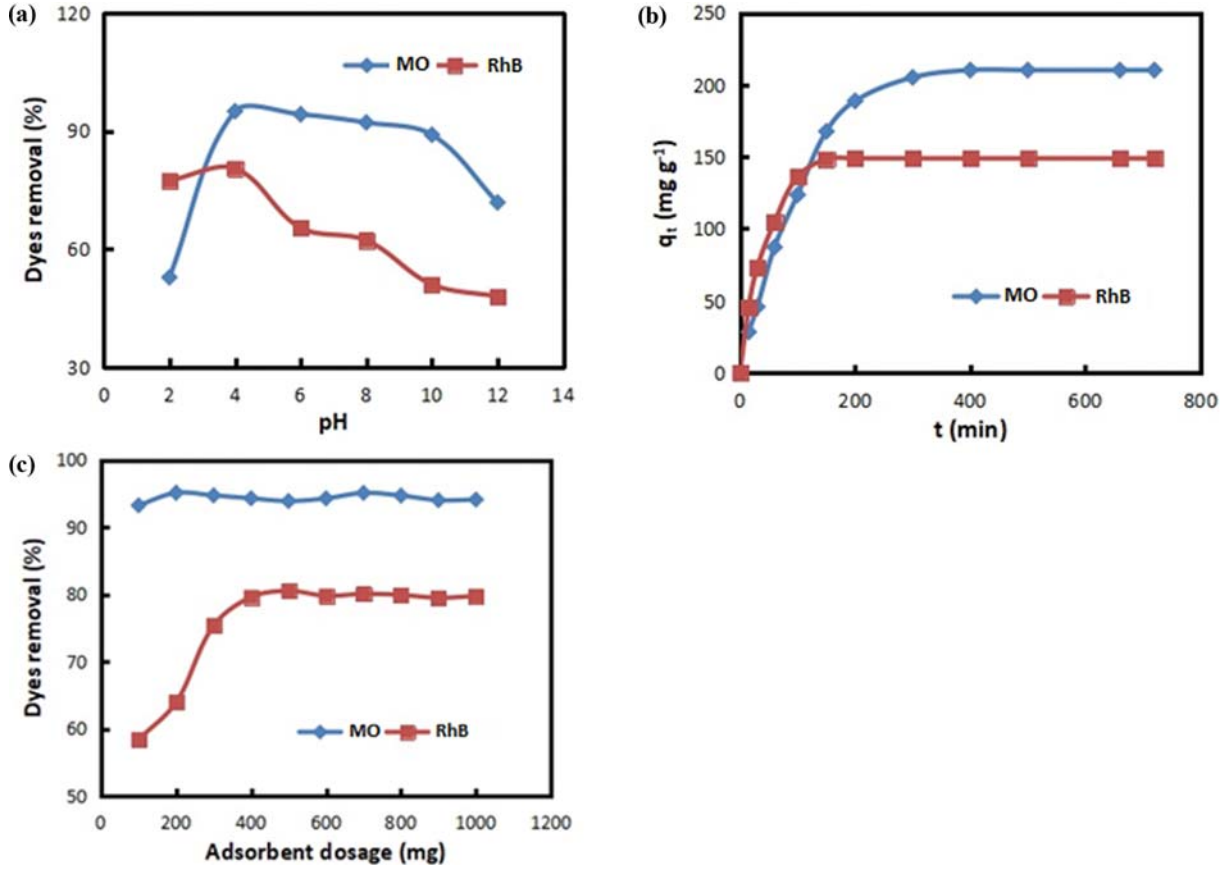

Fig. S1. Effect of (a) pH (b) contact time and (c) adsorbent dosage on the adsorption of MO and RhB onto $LaCoO_3$ at 30 °C.

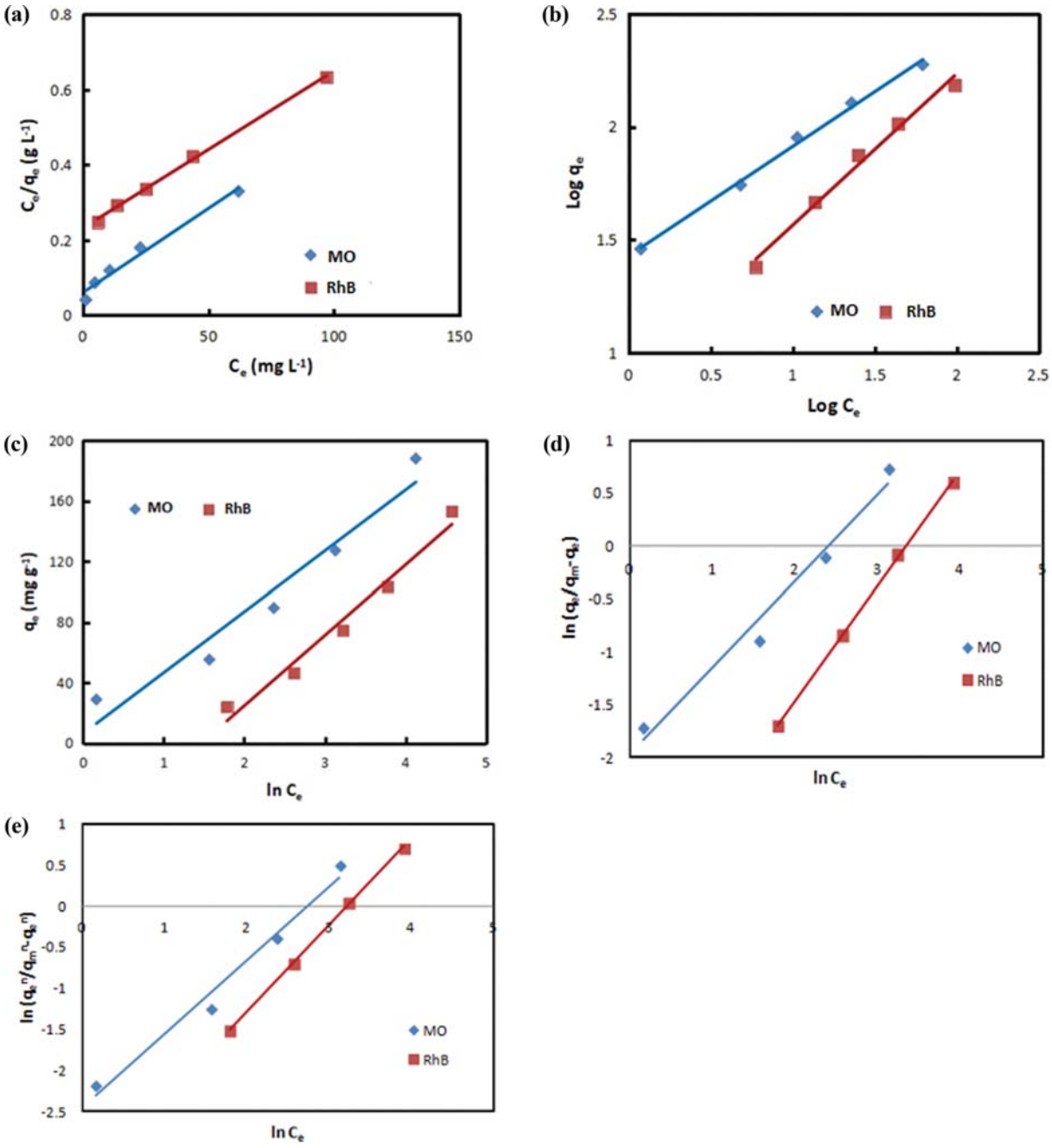

Fig. S2. Equilibrium isotherm models (a) Langmuir (b) Freundlich (c) Temkin (d) Sips and (e) Toth for the adsorptive removal of MO and RhB onto $LaCoO_3$ at 30 °C.

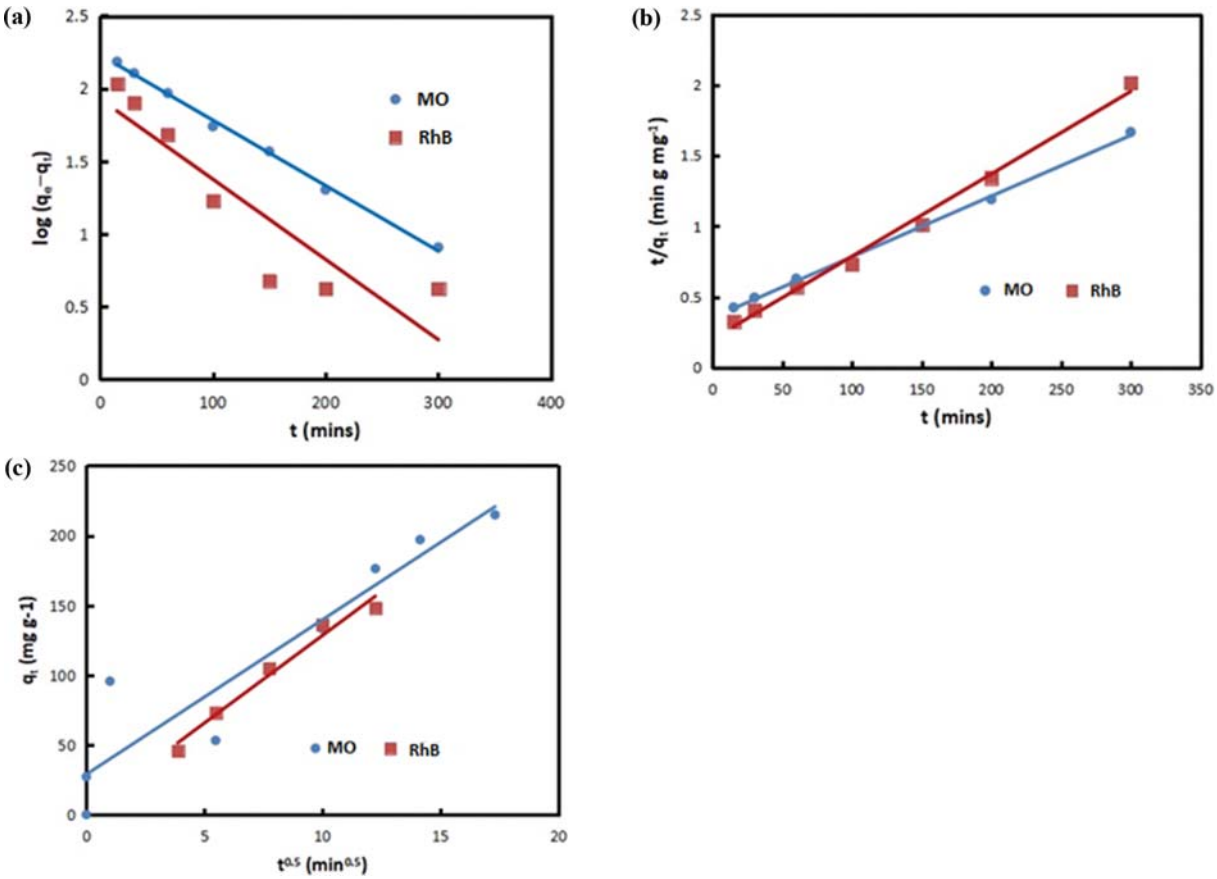

Fig. S3. Kinetic models for the adsorption of MO and RhB onto $LaCoO_3$ at 30 °C (a) pseudo-first order and (b) pseudo-second order (c) intraparticle diffusion kinetic plots.